Biophysical Journal Volume 90 January 2006 589–597

Early Events in Insulin Fibrillization Studied by Time-Lapse Atomic Force Microscopy

Alessandro Podestà,* Guido Tiana,† Paolo Milani,* and Mauro Manno‡

*Istituto Nazionale per la Fisica della Materia, Dipartimento di Fisica, and Cimaina, Università di Milano, Milan, Italy; †Dipartimento di Fisica, Università di Milano and Istituto Nazionale di Fisica Nucleare, Milan, Italy; and ‡Italian National Research Council, Institute of Biophysics at Palermo, Palermo, Italy

ABSTRACT The importance of understanding the mechanism of protein aggregation into insoluble amyloid fibrils lies not only in its medical consequences, but also in its more basic properties of self-organization. The discovery that a large number of uncorrelated proteins can form, under proper conditions, structurally similar fibrils has suggested that the underlying mechanism is a general feature of polypeptide chains. In this work, we address the early events preceding amyloid fibril formation in solutions of zinc-free human insulin incubated at low pH and high temperature. Here, we show by time-lapse atomic force microscopy that a steady-state distribution of protein oligomers with a quasiexponential tail is reached within a few minutes after heating. This metastable phase lasts for a few hours, until fibrillar aggregates are observable. Although for such complex systems different aggregation mechanisms can occur simultaneously, our results indicate that the prefibrillar phase is mainly controlled by a simple coagulation-evaporation kinetic mechanism, in which concentration acts as a critical parameter. These experimental facts, along with the kinetic model used, suggest a critical role for thermal concentration fluctuations in the process of fibril nucleation.

INTRODUCTION

Self-assembly of proteins or peptides into linear elongated structures known as amyloid fibrils is a conserved feature accompanying the clinical manifestation of many pathologies, such as Systemic Amyloidosis or several neurodegenerative diseases (Alzheimer's disease, transmissible spongiform encephalopathy, etc.) (1,2). In several cases, fibril formation is regarded as the onset and the cause of such diseases (''amyloid hypothesis'') (3). More generally, a large number of uncorrelated proteins share the possibility of assembling into similar fibrillar structures under appropriate conditions, which typically favor nonnative conformations (4,5). Therefore, the study of fibrillation kinetics is important for understanding the processes and interactions involved in amyloid self-assembly and designing molecular inhibitors.

The 51-residue hormone insulin has long been known to form fibrils if heated at low pH (6,7), that is, when monomeric or dimeric forms are promoted (8,9). Indeed, insulin is protected from fibrillation by assembling into Zn-hexamers during in vivo storage or in artificial delivery systems (10,11). In acidic conditions, insulin aggregation proceeds mainly via three steps (12–14): formation of active centers (nucleation), elongation of these centers to fibrils (growth), and floccule formation (15). This is a typical scheme for protein polymerization (16) or amyloid formation (17–19). More recently, the structure of insulin fibrils has been shown to resemble that of typical amyloid fibrils with the characteristic cross β-structure (20–23).

To understand the molecular mechanism responsible for the appearance of fibrils, it is necessary to get insight into the early stages of the process. Observation of partially folded intermediate conformations in conditions preceding insulin fibril formation provide a molecular insight into the interactions involved (24–29), yet the onset of aggregation and the causes leading to fibril nucleation and elongation are not clearly understood.

The early stages of fibrillogenesis are, in general, difficult to investigate due to the inherent instability of such systems. Quenching the incubating solution to low temperature allows molecular weight filtering and circular dichroism experiments (30), but the information one obtains concerns conditions different from the incubating ones. Light scattering (18,31) is particularly suited to detect either large supramolecular aggregates or protein-size objects at sufficiently high mass concentration, and consequently it misses the early events in fibrillation kinetics. Neutron scattering has been used to detect small fibrillar precursors (32), but needs long measurements, and thus one can obtain but time-averaged quantities. Atomic force microscopy (AFM) is a technique that can detect fine-grained features of samples deposited on a substrate (the resolution corresponding to the inverse curvature of the tip, which is ~5 nm). Time-lapse AFM has been used extensively to observe the structure and growth of amyloid fibrils (33,34).

In this work, we performed AFM experiments during fibrillation of human insulin. We chose to deposit a small aliquot of incubated solutions, rather than to perform in situ AFM, to avoid the effects of surfaces, which are known to

Submitted June 15, 2005, and accepted for publication October 3, 2005.

Address reprint requests to Mauro Manno, Italian National Research Council, Institute of Biophysics at Palermo, via U. La Malfa 153, 90146 Palermo, Italy. Tel: 39-091-680-9305; Fax: 39-091-680-9349; E-mail: mauro.manno@pa.ibf.cnr.it.

0006-3495/06/01/589/09 $2.00

doi: 10.1529/biophysj.105.068833

affect insulin aggregation (35). In particular, we focused on the early stages preceding the observation of mature fibrils. To explore the lag phase with sufficient time-resolution, we used zinc-free recombinant human insulin, since in this case fibril formation takes place on a timescale of hours (9,29) and it is slower than that of the best studied bovine insulin (36–41). AFM snapshots at different times show a distribution of ellipsoidal oligomeric aggregates, consistent with analogous findings in other amyloidogenic systems, such as the Alzheimer's amyloid β(1–40) peptide (42–45) or other proteins (46,47). After 4 h of incubation, ellipsoidal protein oligomers disappear from AFM images and amyloid fibrils of different length begin to be detected, with a structure analogous to that observed for bovine insulin fibers (23,41). Such changes in aggregate distribution and shape occur within the experiment time resolution of 30 min.

It is unlikely that, for a physical system characterized by such a molecular complexity as a monomer of insulin, a single aggregation mechanism takes place, as in the case of simpler phase transitions, such as liquid crystals. However, one wishes to identify, if it exists, the main driving mechanism which causes the transition from a homogeneous solution of insulin to ordered fibrils.

A primary finding from our experiments is that the oligomer distribution is stationary during the lag-phase and it exhibits an exponential tail. The median values of this distribution are consistent with electrospray mass-spectrometry experiments performed on bovine insulin in analogous conditions (20), but also larger oligomers, up to several tens, are involved. This metastable phase can be explained by a coagulation-evaporation process that has been proposed for colloidal aggregation (48). As to this model, the existence of a stationary oligomer distribution is critically controlled by protein concentration. Consequently, we could argue that small local concentration fluctuations are enough to make the system cross to the dynamical phase characterized by large ''elongated'' growing clusters.

Our work is thus in harmony with experimental observations (49,50) and theoretical studies (51,52) of protein clusters distributions in conditions promoting protein crystallization. Our results shed a new light on the current view of fibril nucleation, suggesting a relevant role for thermal fluctuations and protein-protein interactions leading to cluster formation rather than to physical fibrillar precursors.

MATERIALS AND METHODS

Sample preparation

Recombinant human insulin powder (purchased from Sigma Chemical Co. (St. Louis, MO) and used without further purification) was directly dissolved at 5°C in buffer solution (50 mM KCl/HCl in Millipore SuperQ water, pH 1.6 at 60°C). The protein solution was gently stirred, filtered through a 0.22-mm Millex-GV filter (Millipore, Bedford, MA) into glass cells, and incubated at 60°C. Insulin concentration was 200 μM as measured by ultraviolet absorption at 276 nm using an extinction coefficient of 1.0675 for 1.0 mg/ml. The final concentrations were consistent with those calculated by weighting insulin powder, thus confirming that essentially no material was lost through filtering and that insulin was efficiently dissolved. After given time intervals, 10 μl of incubated protein solution were diluted into 1 ml buffer solution, quenched to 0°C to rapidly inhibit further aggregation, and used for atomic force microscopy experiments. All chemicals were analytical grade.

Atomic force microscopy

A few μl of the insulin solution were dropped onto a freshly cleaved mica substrate (quality ruby muscovite). After a few minutes, the sample was washed dropwise with Millipore SuperQ water, and then dried with a gentle stream of dry nitrogen. Images of the protein aggregates were recorded with a Multimode Nanoscope IIIa AFM (Veeco Instruments, Santa Barbara, CA), operating in tapping mode inside a sealed box where a dry nitrogen atmosphere was maintained. We used rigid cantilevers with resonance frequencies of ~300 kHz and equipped with single crystal silicon tips with nominal radius of curvature 5–10 nm. Typical scan size was 500×500 nm^2 (512×512 points), and scan rate was 1–2 Hz.

Static light scattering

Immediately after preparation, samples were placed in a thermostated cell compartment of a Brookhaven Instruments (Holtsville, NY) BI200-SM goniometer, equipped with a He-Ne laser (wavelength $\lambda_0 = 632.8$ nm). The temperature was set at 60°C and controlled within 0.05°C with a thermostated recirculated bath. Scattered-light intensity at 90° was measured by using a Brookhaven BI-9000 correlator. Absolute values for scattered intensity (Rayleigh ratio) have been obtained by normalization with respect to toluene, whose Rayleigh ratio at 632.8 nm was taken as 14×10^{-6} cm^{-1}.

RESULTS AND DISCUSSION

Time-resolved AFM

Our procedure to investigate early stages of insulin fibrillation consists of incubating the protein in a test tube, extracting samples every 30 min, depositing it on a substrate, and scanning it with the AFM (which takes a time of the order of minutes). The concentration of the protein solution and the incubation time are such that several monolayers of insulin aggregates are deposited onto the mica surface. AFM analysis is carried out on the aggregates belonging to the topmost layer, which are expected not to interact with the mica surface, passivated by the very first monolayers. Moreover, the few minutes of drying of protein samples is expected to remove most of the surface water, while keeping local the protein aggregates substantially hydrated. We exclude therefore the possibility that the protein layers imaged in the dry nitrogen atmosphere are significantly more concentrated than the layers that would assemble on the mica surface in the AFM liquid cell. Thus, we obtain snapshots of the aggregation intermediates until fibrils are formed. Several AFM images of each sample, representative of a given incubation time, were recorded. This allowed collecting the topographic data of $\sim 10^4$ aggregates for each incubation time. Snapshots of the system from the beginning of the incubation (defined as time zero) up to 9 h are displayed in Fig. 1. Such snapshots

indicate that there are oligomers, but not fibril-like structures (cf. Fig. 1, *A–C*), in the first 4 h, until fibrils appear at time 280 min. (cf. Fig. 1, *D–F*). The overall process can thus be divided into a long metastable phase, and the growth of the fibrils. Note that the formation of fibrillar structures is fast compared with the metastable phase, but it is not a sudden critical process, as shown by light-scattering kinetics in Fig. 1 *F*.

AFM data analysis in the early stages of kinetics

A homemade software was used for detecting the edges of the protein aggregates in the AFM maps (A. Podestà, P. Piseri, M. Marino, C. Castelnuovo, and P. Milani, unpublished). The binary maps obtained were then processed using the Image Processing Toolbox of MATLAB (The MathWorks, Natick, MA), and the average distributions of aggregate areas were obtained, as shown in Fig. 2, *A–C*.

Deconvolution of the tip shape from AFM images is a critical issue in any quantitative study of biological samples. Deconvolution algorithms are likely to introduce artifacts in the data, especially when the basic features in the AFM maps are nanometer-sized. Moreover, the morphology of our system, a quasi-two-dimensional close arrangement of nanometer-sized objects, without gaps in between, does not allow the application of simple deconvolution formulas to the distribution of areas (53). These formulas apply to the case of parabolic spherical tips scanning isolated objects lying on a flat reference plane.

We have thus processed raw AFM images without applying any deconvolution. We expect, indeed, reduced convolution

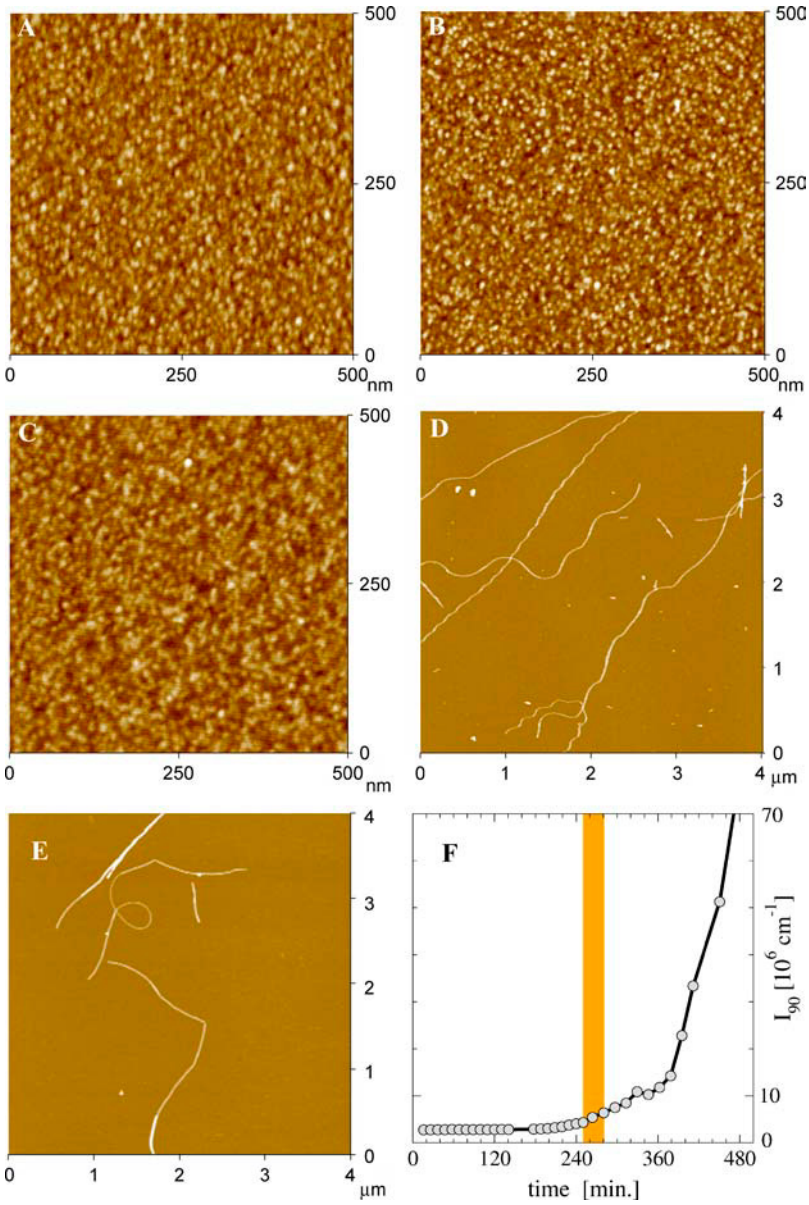

FIGURE 1 (*A–E*) Snapshots of insulin aggregation kinetics at 60°C monitored by kinetic AFM. Times elapsed after incubation: (*A*) 1 min; (*B*) 180 min; (*C*) 250 min; (*D*) 280 min; and (*E*) 540 min. The vertical color scale is 5 nm in *A–C* and 30 nm in *D* and *E*. (*F*) Rayleigh ratio versus time. The colored stripe marks the interval between 250 and 280 min, during which fibrils became observable by AFM.

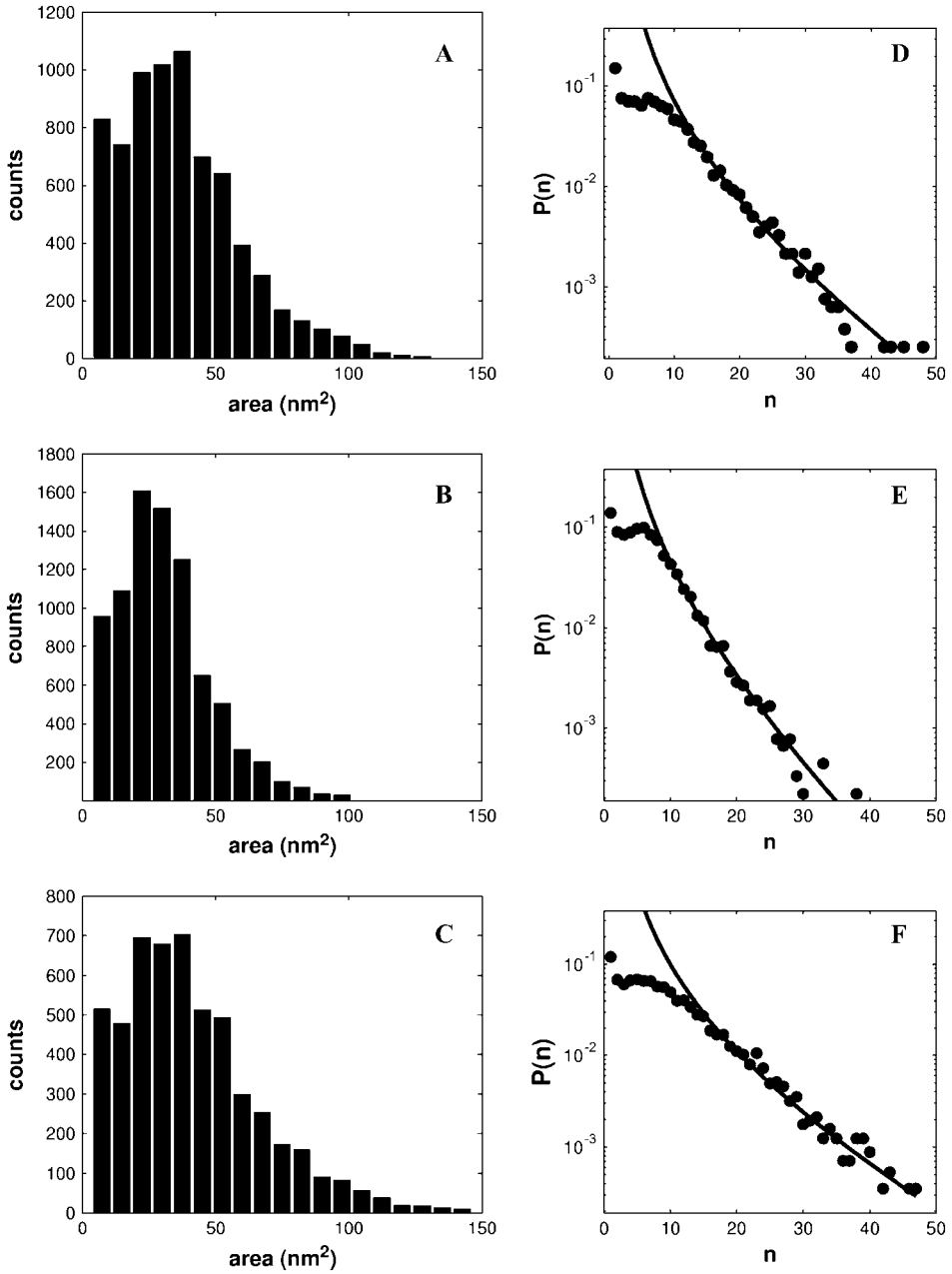

FIGURE 2 Oligomer distributions in the course of kinetics. (*A–C*) Counts of areas observed in AFM images of Fig. 1, *A–C*, respectively. (*D–F*) Frequency of occurrence of aggregation numbers of objects observed in the AFM images of Fig. 1, *A–C*, respectively. Solid lines are fit by Eq. 2.

effects, because the tip does not penetrate deeply down to the substrate but only senses the outermost surface of the protein layer. This insures only negligible lateral contact of the tip and consequently reduced loss of resolution. In addition, the underestimation of the area of the aggregates caused by the erosion of binary maps operated by the edge detection algorithm tends to compensate for the opposite effect produced by the tip shape convolution.

To show that the effects of tip convolution are negligible, we analyzed several AFM images of highly diluted samples, where isolated aggregates lying on the flat mica surface are visible (~20 complexes every 500 × 500 nm^2). These model samples were preprocessed using standard deconvolution algorithms; we used the formula $w' = w - 2(2hR_{tip})^{0.5}$ for a parabolic tip on a step, where R_{tip} is the tip radius (assumed $R_{tip} \sim 3$ nm), h is the step height ($h = \sim 1.1$ nm, the average aggregate height extracted by the AFM images), and w and w' are the apparent and deconvoluted widths of the observed features (53). The resulting distributions of areas were in good agreement with those obtained from the nondeconvoluted raw AFM images (data not shown). In particular, the median and standard deviation of the areas were 27 ± 35 nm^2 accordingly, to be compared with the average values of 30 ± 22 nm^2 extracted from the raw AFM images of concentrated samples.

Quantitative estimation of aggregate size from areas rather than from heights is more reliable because the peculiar vertical interaction of the AFM tip with biological samples usually leads to underestimation of the true height. The same effect is caused by the close packing of insulin aggregates in relatively concentrated samples, which keeps the tip from getting in touch with the flat reference substrate. Processing AFM images of concentrated samples, however, allowed us to collect the large amount of data required to have a stable fit of the area distributions.

Shape of oligomers

The shape of the aggregates can be characterized by means of their eccentricity. The eccentricity of the protein aggregates was also evaluated from the binary maps using the same MATLAB toolbox. Eccentricity is defined as $[1 - (a/b)^2]^{0.5}$, a and b being the minor and major axes, respectively, of the aggregate. This parameter is expected to be 0 for a circle, and 1 for a segment. Correlations of eccentricity and areas are shown in Fig. 3, which shows that even this feature of the system is stationary in the metastable phase. Aggregates have a mean eccentricity of 0.75 that stands for a ratio between large and small axes of ~1.5. Larger aggregates have a larger eccentricity than smaller aggregates, evidencing a preferential one-dimensional (fibrillar) growth for clustering proteins, consistent with recent theoretical findings on colloid clusters with both short-range attraction and long-range repulsion (51,52). Because of the rounding effect of tip convolution, the measured eccentricity is, at most, an underestimate of the actual one.

Average mass of insulin oligomers at the onset of kinetics

Light-scattering experiments were performed immediately after incubation at 60°C. Measurement of the intensity scattered at 90° (scattering vector $q = 18.6\ \mu m^{-1}$) provides the Rayleigh ratio $I_R(q)$, which is related to the weight average molecular mass M_w by the relation $I_R(q) = 4\pi^2\tilde{n}^2(d\tilde{n}/dc)^2 \lambda_0^{-4}N_A^{-1}cM_wP_z(q)$, where c is mass concentration, $\tilde{n}$ is medium refractive index, λ_0 is incident wavelength, N_A is Avogadro's number, and $P_z(q)$ is the z-averaged form factor (31). By taking $(d\tilde{n}/dc) = 0.18\ cm^3\ g^{-1}$, and $P_z(q) = 1$ (since the initial size of solutes is much smaller than q^{-1}), we obtain an average molecular mass of 10 ± 2 kDa. Considering that the molecular mass of a single insulin molecule is 5806 Da, the mean average aggregation number of insulin oligomers found at the onset of kinetics is 1.7 ± 0.3. Note, however, that the latter value, obtained by light-scattering measurements, corresponds to the ratio between the second and the first moment of oligomer distribution (31), and gives no information on the actual distribution shape.

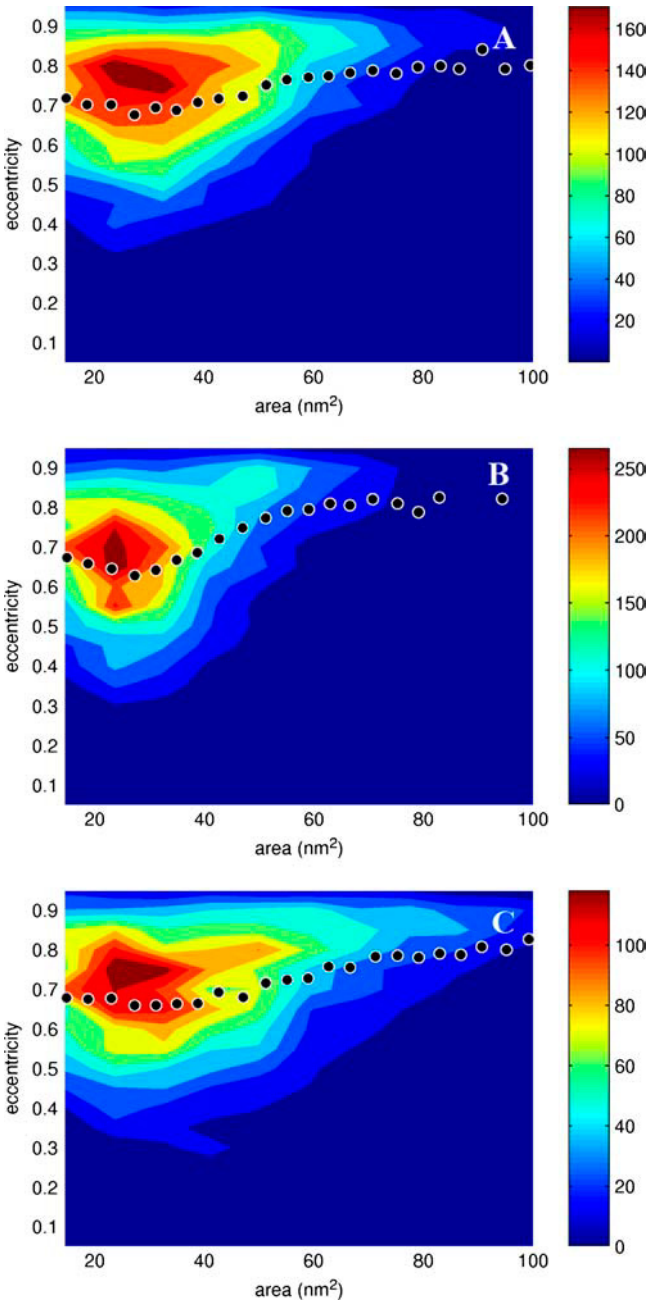

FIGURE 3 Size-eccentricity correlation. (*A–C*) Correlation of eccentricity and areas of objects observed in the AFM images of Fig. 1, *A–C*, respectively. Dotted curves represent average eccentricity versus aggregate area.

Oligomer distribution preceding amyloid formation

Volumes of imaged objects were derived from calculated areas and eccentricities, under the assumption that the aggregates are prolate ellipsoids. Aggregation numbers, n, are obtained by using the relation $V = V_0n^{1/d}$, where $V_0 = 14.1\ nm^3$ is the van der Waals volume of an insulin monomer, including a layer of water, derived from the x-ray structure

(54), and $d = 2.68$ is an effective fractal dimension that accounts for the scaling between mass and size of aggregates. The value $d = 2.68$ is derived from x rays and light-scattering data (54–56) on oligomers of zinc-free insulin at high pH. Note that zinc-free insulin is not tightly packed nor is it assembled into toroid-shaped hexamers like zinc insulin. We have found that by assuming an effective fractal dimension between 2 (enough loose aggregates) and 3 (space-filling objects), the shape of oligomer distribution is not significantly altered, that is, the distribution shape is robust with respect to different reasonable choice of molecular packing. This distribution implies that aggregates built from up to 50 monomers are detectable in the initial stages of aggregation. The large size of these oligomers is in agreement with the micellar precursors identified in Lomakin et al. (18) in the case of Alzheimer's amyloid β-peptide.

The distribution of oligomer aggregation numbers at different times in the metastable phase is displayed in Fig. 2, *D–F*. All the curves well overlap, indicating that the distribution of size is stationary. The median aggregation numbers, n_m, are 5.9, 4.9, and 6.7, respectively, for the three cases shown in the figure. The tail of such distributions can be fit by an exponential of the kind $\exp(-n/n_m)$ (cf. Fig. 2), where n_m is the median aggregation number.

Note that according to the kinetic model described, as well as to the light-scattering results, the majority of the protein should be in the monomeric or dimeric form. However, it is not surprising that such small species are hidden in the crowded AFM images, or confused among the smallest fragments in the binary maps of aggregates generated by the edge-detection algorithm, and thus filtered out. Consistently, we afford a statistical analysis of oligomer distribution by considering only the higher concentration numbers.

Kinetic model for oligomer distribution

The most evident feature of the distributions of oligomer size and aggregation number shown in Fig. 2 is that they reach a steady state within the time detectable from the experiment (i.e., a few minutes). A steady state means that, unlike diffusion-limited or reaction-limited mechanisms, which regulate the assembly of larger aggregates (19), in this case we deal with an ''evaporation'' process (i.e., monomers leaving the aggregates), which competes with ''coagulation''. To perform AFM experiments, samples have been manipulated by the procedures described above. In particular, sample dilutions alter profoundly the initial thermodynamic conditions. However, such intrinsic weakness of the experimental approach confirms that the observed distribution is due to a kinetic coagulation process. Indeed, by applying bare thermodynamic equilibrium between different oligomeric species, one would expect that upon such dilution insulin would be essentially monomeric (8).

A mechanism for protein association that accounts for both aggregation and evaporation processes can be outlined in the framework of classical coagulation theory (57). If we call $\rho_n(t)$ the number concentration of aggregates built out of n monomers at time t, the rate equation of the system reads:

$$\frac{d}{dt}\rho_n(t) = \sum_{\substack{i=1\\(n>1)}}^{n-1} K_{i(n-i)}\,\rho_i(t)\,\rho_{(n-i)}(t) - \rho_n(t)\sum_{j=1}^{\infty} K_{nj}\,\rho_j(t) + \lambda_{n+1}\rho_{n+1}(t) - \lambda_n\rho_n(t) + \delta_{n1}\sum_{j=1}^{\infty}\lambda_j\,\rho_j(t), \quad (1)$$

where $\delta_{ij} = 1$ for $i = j$, and zero otherwise. The first two terms in the right-hand side of the latter equation are, respectively, the production and loss of n-mers by coagulation of two clusters of i and j proteins, whereas the other terms describe the ''evaporation'' of one monomer from a cluster of $n + 1$ proteins into a cluster of n proteins and a single protein. Here, we include no nucleation term, and we also assume that three-body effects can be ignored.

The simplest solution of such equations has been provided by Krapivsky and Redner (48) by taking mass independent rate constants, $K_{ij} = K$ and $\lambda_i = \lambda$, and assuming that only monomers are present at time zero, that is $\rho_n(0) = cM_0^{-1}\delta_{n1}$, where c is the total mass concentration and M_0 is the mass of a monomer.

The model displays two behaviors, controlled by the parameter $\mu = K\lambda^{-1}cM_0^{-1}$, that is, by the ratio between the coagulation and evaporation rate constants and by the initial concentration of monomers. At low protein concentration ($\mu < 1$) the system displays a steady-state distribution $P(n) = \rho_n/\Sigma\rho_n$ with an asymptotic tail that is an exponential times a power law:

$$P(n) = x^{n-1}\frac{\Gamma(n-\frac{1}{2})}{\Gamma(n+1)\Gamma(\frac{1}{2})}\left[1 - \frac{n-\frac{1}{2}}{n+1}x\right], \quad (2)$$

where $x = \mu(2 - \mu)$. At $\mu = 1$, the system displays a power-law distribution, whereas at higher concentrations ($\mu > 1$) it does not display any steady state, the typical cluster growing linearly in time.

The tails of the distributions shown in Fig. 2, *D–F*, are well fit by Eq. 2, indicating that the system is in the low-concentration regime. For the three distributions, one obtains, respectively, $\mu = 0.71$, 0.66, and 0.73. The mass averaged mean aggregation number n_z, which is accessible through scattering experiments and is found to be 1.7 ± 0.3, can be expressed in terms of this model as the ratio between the second and the first moment of the distribution: $n_z = (1 - \mu)^{-1} = 3.3 \pm 0.4$. This slight discrepancy between light-scattering and AFM results points out the lack of monomeric and dimeric oligomers from AFM images, as discussed above. Also, note that a simple-minded exponential (maximum-entropy) distribution would give a worse fit and a much higher mass averaged mean aggregation number ($n_z = 11.6 \pm 1.9$).

Due to the large value observed for the parameter μ, one could speculate that local fluctuations in the density of monomers could be the triggering mechanism behind the onset of

fibril formation, akin to that proposed for crystal nucleation (58,59). Note that this does not imply a break of symmetry, since the metastable aggregates already display a pronounced eccentricity.

The kinetic model used needs no assumption concerning thermodynamic equilibrium. Also, the experimental procedure alters the initial thermodynamic conditions. Notwithstanding, it is interesting to consider the free-energy change involved in the clustering process if one assumes a ''metastable'' equilibrium condition. In particular, one can define the free energy ΔG_n associated with the addition of one monomer to a cluster of n proteins, as $\Delta G_n = -k_B T \ln(f_{n+1}/f_n f_1)$, where k_B is the Boltzmann constant and f_n is the activity of a cluster of n proteins. If we take the activity as $f_n = c_n/c$, with c_n the mass concentration of the n-mers and c the total concentration, we obtain for an infinitely large cluster

$$\frac{\Delta G_\infty}{k_B T} = -\ln \frac{2\mu}{1 - \frac{1}{4}\mu(2-\mu)}. \quad (3)$$

From our analysis, we obtained $\Delta G_\infty = -0.6\ k_B T$. Therefore, the free energy related to the growth of a large cluster or fiber is easily accessible through thermal fluctuations. This gives a rationale for the fact that in insulin, as well as in other protein solutions, a change in temperature or in solvent conditions can trigger fibril formation (60).

CONCLUSION

In this work, the early stages of human insulin fibrillation have been monitored by time-lapse AFM, a technique with high resolution and sensitivity. Experimental observations and theoretical modeling highlight an interesting scenario of the nucleation mechanism preceding amyloid fibrillation:

1. Experiments show that, within the limits of resolution of the AFM, a steady-state distribution of protein oligomers with an exponential tail is present in solution up to the point of formation of amyloid fibrils (Figs. 1 and 2).
2. Oligomer distribution can be explained by a kinetic model that combines coagulation and evaporation events (Fig. 2, *D–F*). As to this model, the formation of ''nonstationary'', growing aggregates is controlled by monomer concentration. In this case, concentration is below the critical value, yet sufficiently high to allow ''above-threshold'' thermal concentration fluctuations. It should be remarked that although our scheme captures an interesting feature of insulin aggregation, its generalization to different thermodynamic conditions and concentrations is not straightforward due to the complex hierarchy of structures and processes involved (34).
3. Prefibrillar oligomers exhibit a marked eccentricity (Fig. 3), denoting that the symmetry breaking implied by the existence of fibrillar aggregates has already occurred before fibrillation. Indeed, it is reasonably related to a ''fast'' conformational change (22,25,29). From the latter experimental results, we can argue that such oligomers are actual ''on-pathway'' intermediates of mature fibrils.

The appearance of mature amyloid fibrils seems fast when compared with the duration of the lag phase and if detected within the time resolution of the experiments, which is 30 min. However, it is not a critical process, as shown by the kinetics of Fig. 1 *F*. The details of the actual mechanism of fibril formation are not visible in the main structural information obtained by AFM experiments. Indeed, the observations presented here enable us to grasp the main structural features of the mechanism controlling the size of the objects in solution during the lag phase. Also, along with the extremely naïve model used, they show that these aggregates are formed by a kinetic process.

The existence of prefibrillar precursors acting as aggregation nuclei has been widely observed in amyloid formation both as preexisting seeds and as actual self-assembled nuclei (17). Our results point out that, along with the existence of such precursors, local density fluctuations may play a critical role in the nucleation mechanism and trigger amyloid fibrillogenesis.

We gratefully acknowledge the help of L. Finzi. We thank E. Craparo, D. Bulone, V. Martorana, P. L. San Biagio, C. Rishel, and F. Librizzi for collaboration and for access to unpublished data.

This work was partially supported by the Italian Ministero della Salute through the projects ''Neuropatie animali-analisi molecolari e funzionali della proteina prionica in razze bovine siciliane'' and ''Deposito della beta amiloide nella membrana cellulare - ruolo degli ioni metallici e dei radicali liberi''.

REFERENCES

1. Rochet, J. C., and P. T. Lansbury, Jr. 2000. Amyloid fibrillogenesis: themes and variations. *Curr. Opin. Struct. Biol.* 10:60–68.
2. Kelly, J. W. 1996. Alternative conformations of amyloidogenic proteins govern their behavior. *Curr. Opin. Struct. Biol.* 6:11–17.
3. Hardy, J., and D. J. Selkoe. 2002. The amyloid hypothesis of Alzheimer's disease: progress and problems on the road to theurapetics. *Science*. 297:353–356.
4. Chiti, F., P. Webster, N. Taddei, A. Clark, M. Stefani, G. Ramponi, and C. M. Dobson. 2002. Designing conditions for *in vitro* formation of amyloid protofilaments and fibrils. *Proc. Natl. Acad. Sci. USA*. 96: 3590–3594.
5. Stefani, M., and C. M. Dobson. 2003. Protein aggregation and aggregate toxicity: new insights into protein folding, misfolding diseases and biological evolution. *J. Mol. Med.* 81:678–699.
6. Langmuir, I., and D. F. Waugh. 1940. Pressure-soluble and pressure-displaceable components of monolayers of native and denatured proteins. *J. Am. Chem. Soc.* 62:2771–2793.
7. Waugh, D. F. 1944. The linkage of corpuscular protein molecules. I. A fibrous modification of insulin. *J. Am. Chem. Soc.* 66:663–663.
8. Doty, P., and G. E. Myers. 1953. II. Low molecular weight proteins. Thermodynamics of the association of insulin molecules. *Discuss. Faraday Soc.* 13:51–58.
9. Brange, J., L. Andersen, E. D. Laursen, G. Meyn, and E. Rasmussen. 1997. Towards understanding insulin fibrillation. *J. Pharm. Sci.* 86: 517–525.
10. Brange, J. 1987. Galenics of Insulin: The Physico-Chemical and Pharmaceutical Aspects of Insulin and Insulin Preparations. Springer-Verlag, Berlin.

11. Lougheed, W. D., H. Woulfe-Flanagan, J. R. Clement, and A. M. Albisser. 1980. Insulin aggregation in artificial delivery systems. *Diabetologia*. 19:1–9.
12. Waugh, D. F., D. F. Wilhemson, S. L. Commerford, and M. L. Sackler. 1953. Studies of the nucleation and growth reactions of selected types of insulin fibrils. *J. Am. Chem. Soc.* 75:2592–2600.
13. Waugh, D. F. 1954. Protein-protein interactions. *Adv. Protein Chem.* 9:352–437.
14. Waugh, D. F. 1957. A mechanism for the formation of fibrils from protein molecules. *J. Cell. Comp. Physiol.* 49:145–164.
15. Krebs, M. R. H., C. E. MacPhee, A. F. Miller, I. E. Dunlop, C. M. Dobson, and A. M. Donald. 2004. The formation of spherulites by amyloid fibrils of bovine insulin. *Proc. Natl. Acad. Sci. USA*. 101: 14420–14424.
16. Oosawa, F., and S. Asakura. 1975. Thermodynamics of the Polymerization of Proteins. Academic Press, London.
17. Harper, J. D., and P. T. Lansbury, Jr.. 1997. Models of amyloid seeding in Alzheimer's disease and scrapie: mechanistic truths and physiological consequences of the time-dependent solubility of amyloid proteins. *Annu. Rev. Biochem.* 66:385–407.
18. Lomakin, A., D. S. Chung, G. B. Benedek, D. A. Kirschner, and D. B. Teplow. 1996. On the nucleation and growth of amyloid β-protein fibrils: detection of nuclei and quantitation of rate constants. *Proc. Natl. Acad. Sci. USA*. 93:1125–1129.
19. Lomakin, A., D. B. Teplow, D. A. Kirschner, and G. B. Benedek. 1997. Kinetic theory of fibrillogenesis of amyloid β-protein. *Proc. Natl. Acad. Sci. USA*. 94:7942–7947.
20. Nettleton, E. J., P. Tito, M. Sunde, M. Bouchard, C. M. Dobson, and C. V. Robinson. 2000. Characterization of the oligomeric states of insulin in self-assembly and amyloid fibril formation by mass spectroscopy. *Biophys. J.* 79:1053–1065.
21. Bouchard, M., J. Zurdo, E. J. Nettleton, C. M. Dobson, and C. V. Robinson. 2000. Formation of insulin amyloid fibrils followed by FTIR simultaneously with CD and electron microscopy. *Protein Sci.* 9: 1960–1967.
22. Tito, P., E. J. Nettleton, and C. V. Robinson. 2000. Dissecting the hydrogen exchange properties of insulin under amyloid fibril forming conditions: A site-specific investigation by mass spectroscopy. *J. Mol. Biol.* 303:267–278.
23. Jimenez, J. L., E. J. Nettleton, M. Bouchard, C. V. Robinson, C. M. Dobson, and H. R. Saibil. 2000. The protofilament structure of insulin amyloid fibrils. *Protein Sci.* 9:1960–1967.
24. Hua, Q.-X., and M. A. Weiss. 1991. Comparative 2D NMR studies of human insulin and des-pentapeptide insulin: Sequential resonance assignment and implication for protein dynamics and receptor recognition. *Biochemistry.* 30:5505–5515.
25. Brange, J., G. G. Dodson, D. J. Edwards, P. H. Holdon, and J. L. Whittingham. 1997. A model of insulin fibrils derived from the x-ray crystal structure of a monomeric insulin (despentapeptide insulin). *Proteins*. 27:507–516.
26. Whittingham, J. L., D. J. Scott, K. Chance, A. Wilson, J. Finch, J. Brange, and G. G. Dodson. 2002. Insulin at pH 2: Structural analysis of the conditions promoting insulin fibre formation. *J. Mol. Biol.* 318: 479–490.
27. Ahmad, A., I. S. Millett, S. Doniach, V. N. Uversky, and A. L. Fink. 2003. Partially folded intermediates in insulin fibrillation. *Biochemistry.* 42:11404–11416.
28. Ahmad, A., I. S. Millett, S. Doniach, V. N. Uversky, and A. L. Fink. 2004. Stimulation of insulin fibrillation by urea-induced intermediates. *J. Biol. Chem.* 279:14999–15013.
29. Hua, Q.-X., and M. A. Weiss. 2004. Mechanism of insulin fibrillation: The structure of insulin under amyloidogenic conditions resembles a protein-folding intermediate. *J. Biol. Chem.* 279:21449–21460.
30. Jarvet, J., P. Damberg, K. Bodell, L. E. G. Eriksson, and A. Gräslund. 2000. Reversible random coil to β-sheet transition and the early stage of aggregation of the A(12–28) fragment from the Alzheimer peptide. *J. Am. Chem. Soc.* 122:4261–4268.
31. Carrotta, R., M. Manno, V. Martorana, D. Bulone, and P. L. San Biagio. 2005. Protofibril formation of amyloid β-protein at low pH via a non-cooperative elongation mechanism. *J. Biol. Chem.* 280:30001–30008.
32. Yong, W., A. Lomakin, M. D. Kirkitadze, D. B. Teplow, S.-H. Chen, and G. B. Benedek. 2002. Structure determination of micelle-like intermediates in amyloid β-protein fibril assembly using small angle neutron scattering. *Proc. Natl. Acad. Sci. USA*. 99:150–154.
33. Goldsbury, C., U. Aebi, and P. Frey. 2001. Visualizing the growth of Alzheimer's β amyloid-like fibrils. *Trends Mol. Med.* 7:582.
34. Khurana, R., C. Ionescu-Zanetti, M. Pope, J. Li, L. Nielsen, M. Ramirez-Alvarado, L. Regan, A. L. Fink, and S. A. Carter. 2003. A general model for amyloid fibril assembly based on morphological studies using atomic force microscopy. *Biophys. J.* 85:1135–1144.
35. Sluzky, V., J. A. Tamada, A. Klibanov, and R. Langer. 1991. Kinetics of insulin aggregation in aqueous solutions upon agitation in the presence of hydrophobic surfaces. *Proc. Natl. Acad. Sci. USA*. 88: 9377–9381.
36. Nielsen, L., R. Khurana, A. Coats, S. Frokjaer, J. Brange, S. Vyas, V. N. Uversky, and A. L. Fink. 2001. Effect of environmental factors on the kinetics of insulin fibril formation: elucidation of the molecular mechanism. *Biochemistry.* 40:6036–6046.
37. Nielsen, L., S. Frokjaer, J. Brange, V. N. Uversky, and A. L. Fink. 2001. Probing the mechanism of insulin fibril formation with insulin mutants. *Biochemistry.* 40:8397–8409.
38. Nielsen, L., S. Frokjaer, J. Carpenter, and J. Brange. 2001. Studies of the structure of insulin fibrils by Fourier transform infrared (FTIR) spectroscopy and electron microscopy. *J. Pharm. Sci.* 90:29–37.
39. Dzwolak, W., R. Ravindra, J. Lendermann, and R. Winter. 2004. Aggregation of bovine insulin probed by DSC/PPC calorimetry and FTIR spectroscopy. *Biochemistry.* 42:11347–11355.
40. Jansen, R., S. Grudzielanek, W. Dzwolak, and R. Winter. 2004. High pressure promotes circularly shaped insulin amyloid. *J. Mol. Biol.* 338:203–206.
41. Jansen, R., W. Dzwolak, and R. Winter. 2004. Amyloidogenic self-assembly of insulin aggregates probed by high resolution atomic force microscopy. *Biophys. J.* 88:1344–1353.
42. Walsh, D. M., A. Lomakin, G. B. Benedek, M. M. Condron, and D. B. Teplow. 1997. Amyloid β-protein fibrillogenesis: detection of a protofibrillar intermediate. *J. Biol. Chem.* 272:22364–22372.
43. Huang, T. H. J., D.-S. Yang, N. P. Plaskos, S. Go, C. M. Yip, P. E. Fraser, and A. Chakrabartty. 2000. Structural studies of soluble oligomers of the Alzheimer β-Amyloid Peptide. *J. Mol. Biol.* 297: 73–87.
44. Westlind-Danielsson, A., and G. Arnerup. 2001. Spontaneous in vitro formation of supramolecular β-amyloid structures, ''βamy balls'', by β-amyloid 1–40 peptide. *Biochemistry.* 40:14736–14743.
45. Hoshi, M., M. Sato, S. Matsumoto, A. Noguchi, K. Yasutake, N. Yoshida, and K. Sato. 2003. Spherical aggregates of β-amyloid (amylospheroid) show high neurotoxicity and activate tau protein kinase I/glycogen synthase kinase-3β. *Proc. Natl. Acad. Sci. USA.* 100:6370–6375.
46. Relini, A., S. Torrassa, R. Rolandi, A. Gliozzi, C. Rosano, C. Canale, M. Bolognesi, G. Plakoutsi, M. Bucciantini, F. Chiti, and M. Stefani. 2004. Monitoring the process of HypF fibrillization and liposome permeabilization by protofibrils. *J. Mol. Biol.* 338:943–957.
47. Xu, S., B. Bevis, and M. F. Arnsdorf. 2001. The assembly of amyloidogenic Yest Sup35 as assessed by scanning (atomic) force microscopy: an analogy to linear colloidal aggregation? *Biophys. J.* 81:446–454.
48. Krapivsky, P. L., and S. Redner. 1996. Transitional aggregation kinetics in dry and damp environments. *Phys. Rev. E.* 54:3553–3561.
49. Piazza, R., and S. Iacopini. 2002. Transient clustering in a protein solution. *Eur. Phys. J. E.* 7:45–48.

50. Stradner, A., H. Sedgwick, F. Cardinaux, W. C. K. Poon, S. U. Egelhaaf, and P. Schurtenberger. 2004. Equilibrium cluster formation in concentrated protein solution and colloids. *Nature*. 432:492–495.

51. Sciortino, F., S. Mossa, E. Zaccarelli, and P. Tartaglia. 2004. Equilibrium cluster phases and low-density arrested disordered states: the role of short-range attraction and long-range repulsion. *Phys. Rev. Lett*. 93:055701.

52. Mossa, S., F. Sciortino, P. Tartaglia, and E. Zaccarelli. 2005. Ground state clusters for short-range attractive and long-range repulsive potentials. *Langmuir*. 20:10756–10763.

53. Odin, C., J. P. Aimeé, Z. El Kaakour, and T. Bouhacina. 1994. Tip finite size effects on atomic force microscopy in the contact mode: simple geometrical considerations for rapid estimation of apex radius and tip angle based on the study of polystyrene latex ball. *Surf. Sci*. 317:321–340.

54. Baker, E. N., T. L. Blundell, J. F. Cutfield, S. M. Cutfield, E. J. Dodson, G. G. Dodson, D. M. Crowfoot Hodgkin, R. E. Hubbard, N. W. Isaacs, C. D. Reynolds, K. Sakabe, N. Sakabe, and N. M. Vijayan. 1988. The structure of 2Zn pig insulin crystals at 1.5 Å resolution. *Philos. Trans. R. Soc. Lond. B Biol. Sci*. 319:369–456.

55. Kadima, W., L. Ogendal, R. Bauer, N. Kaarsholm, K. Brodersen, J. F. Hansen, and P. Porting. 1993. The influence of ionic strength and pH on the aggregation properties of zinc-free insulin studied by static and dynamic laser light scattering. *Biopolymers*. 33:1643–1657.

56. Pedersen, J. S., S. Hansen, and R. Bauer. 1994. The aggregation behavior of zinc-free insulin studied by small-angle neutron scattering. *Eur. Biophys. J*. 22:379–389.

57. Chandrasekhar, S. 1943. Stochastic problems in physics and astronomy. *Rev. Mod. Phys*. 15:1–89.

58. ten Wolde, P. R., and D. Frenkel. 1997. Enhancement of protein crystal nucleation by critical density fluctuations. *Science*. 277:1975–1978.

59. Manno, M., D. Bulone, V. Martorana, and P. L. San Biagio. 2004. Thermodynamic instability and off-critical slowing down in supersaturated lysozyme solutions. *J. Phys. Condens. Matter*. 16:S5023–S5033.

60. Manno, M., P. L. San Biagio, and M. U. Palma. 2004. The role of pH on instability and aggregation of sickle hemoglobin solutions. *Proteins*. 55:169–176.